

THE QUADRUPLE PRE-MAIN SEQUENCE SYSTEM LkCa 3: IMPLICATIONS FOR STELLAR EVOLUTION MODELS

GUILLERMO TORRES¹, DARY RUÍZ-RODRÍGUEZ², MARIONA BADENAS³, L. PRATO², G. H. SCHAEFER⁴, LAWRENCE H. WASSERMAN², ROBERT D. MATHIEU⁵, AND DAVID W. LATHAM¹

Accepted for publication in the Astrophysical Journal

ABSTRACT

We report the discovery that the pre-main sequence object LkCa 3 in the Taurus-Auriga star-forming region is a hierarchical quadruple system of M stars. It was previously known to be a close ($\sim 0''.5$) visual pair, with one component being a moderately eccentric 12.94-day single-lined spectroscopic binary. A re-analysis of archival optical spectra complemented with new near-infrared spectroscopy shows both visual components to be double-lined, the second one having a period of 4.06 days and a circular orbit. In addition to the orbital elements, we determine optical and near-infrared flux ratios, effective temperatures, and projected rotational velocities for all four stars. Using existing photometric monitoring observations of the system that had previously revealed the rotational period of the primary in the longer-period binary, we detect also the rotational signal of the primary in the 4.06-day binary, which is synchronized with the orbital motion. With only the assumption of coevality, a comparison of all of these constraints with current stellar evolution models from the Dartmouth series points to an age of 1.4 Myr and a distance of 133 pc, consistent with previous estimates for the region and suggesting the system is on the near side of the Taurus complex. Similar comparisons of the properties of LkCa 3 and of the well-known quadruple pre-main sequence system GG Tau with the widely used models from the Lyon series for a mixing length parameter of $\alpha_{ML} = 1.0$ strongly favor the Dartmouth models.

Subject headings: binaries: close — binaries: spectroscopic — stars: individual (LkCa 3) — stars: pre-main-sequence — stars: rotation — techniques: radial velocities

1. INTRODUCTION

The study of multiplicity among pre-main sequence (PMS) stars is of key importance to our understanding of the process of star formation, and to interpret the observed multiplicities of normal stars in the solar neighborhood, which are evolved from the younger populations. A recent review of stellar multiplicity by Duchêne & Kraus (2013) noted that while imaging surveys of PMS stars by many teams have turned up significant numbers of visual binaries, our knowledge of tighter systems typically discovered in spectroscopic surveys is considerably more incomplete among young stars. This is unfortunate, as close binaries for which the orbital elements are known provide very useful constraints on star formation theory from the distributions of their mass ratios (e.g., Bate 2009), as well as their periods and other properties. They also present an opportunity to improve our understanding of tidal circularization theory (Zahn & Bouchet 1989; Mathieu et al. 1992; Melo et al. 2001; Witte & Savonije 2002; Meibom & Mathieu 2005; Mazeh 2008). Importantly, in favorable cases they allow the determination of the dynamical masses of the components, which are essential for testing models of stellar

evolution for young stars (see, e.g., Hillenbrand & White 2004; Mathieu et al. 2007; Simon 2008). Relatively few PMS stars have this information available, and as a result evolution models for young stars are much more poorly constrained than those for their main-sequence counterparts.

An account of our state of knowledge about multiple systems among PMS stars by Mathieu (1994) listed a grand total of 25 spectroscopic binaries for which orbits had been established, of which half were unpublished at the time. Since then relatively few long-term spectroscopic surveys have been carried out (e.g., Covino et al. 2001; Melo 2003; Prato 2007; Guenther et al. 2007; Nguyen et al. 2012), and while some have produced new systems with orbital solutions, most additions to the list of binaries with known orbits have come from serendipitous discoveries. Slightly more than half of the known PMS spectroscopic binaries are double-lined, which are especially valuable in that they provide mass ratios. In recent years significant efforts have been carried out with good success to detect the faint secondaries of some of the single-lined systems by observing in the near infrared (NIR), where the contrast is more favorable (e.g., Mazeh et al. 2002; Prato et al. 2002a,b; Mace et al. 2012; Simon et al. 2013).

LkCa 3 (also V1098 Tau, 2MASS J04144797+2752346, HBC 368) was listed by Mathieu (1994) as a single-lined spectroscopic binary in the Taurus-Auriga star-forming region with an orbital period of 12.941 days and an eccentricity of 0.20, although the particulars of the orbital solution were not reported there. It was also known at the time to be a visual binary with an angular separation of $0''.47$ (Leinert et al. 1993), implying a hierarchical

¹ Harvard-Smithsonian Center for Astrophysics, 60 Garden St., Cambridge, MA 02138, USA; e-mail: gtorres@cfa.harvard.edu

² Lowell Observatory, 1400 West Mars Hill Road, Flagstaff, AZ 86001, USA

³ Department of Astronomy, Yale University, New Haven, CT 06520, USA

⁴ The CHARA Array of Georgia State University, Mount Wilson Observatory, Mount Wilson, CA 91023, USA

⁵ Department of Astronomy, University of Wisconsin-Madison, Madison, WI 53706, USA

configuration of at least three stars assuming the visual components are physically associated. Its PMS status was established earlier by Herbig et al. (1986) on the basis of its strong Ca II H and K emission and the presence of the Li I $\lambda 6707$ line in absorption. Its spectral type is most often listed as M1, and from the strength of the H α emission line ($\sim 2.5 \text{ \AA}$ equivalent width; Hartmann et al. 1987) it is considered a weak-line T Tauri star (WTTS). No infrared excess or sub-millimeter emission has been observed (e.g., Simon & Prato 1995; Dutrey et al. 1996; Stassun et al. 2001; Andrews & Williams 2005), consistent with the absence of any appreciable surrounding disk material.

Beyond their initial use by Mathieu (1994) to report the discovery of LkCa 3 as a single-lined spectroscopic binary, the original spectra of this object have not been exploited to the fullest extent now possible with the significant improvements in spectroscopic analysis techniques that have taken place in the intervening years. This has prompted us to revisit the system. The motivation for this paper is the discovery that LkCa 3 is in fact a hierarchical quadruple system, in which each of the visual components is a double-lined spectroscopic binary. Full details of the orbital solutions are presented, which incorporate not only the archival spectroscopic material gathered by Mathieu (1994) but also near-infrared spectroscopy obtained more recently that spatially resolves the visual pair. LkCa 3 thus joins the small group of double-lined PMS systems with well-established orbits, contributing two new entries to the list.

The quadruple nature of the system enables much stronger tests of PMS models than would otherwise be possible. We take advantage of this opportunity here. Our spectroscopic observations, along with additional high-resolution imaging we have acquired to better characterize the visual binary, allow us to infer the key physical properties of the four stars in the system by comparison with current models of stellar evolution, including an independent estimate of the distance.

2. OBSERVATIONS

2.1. Optical spectroscopy

The visible-light spectroscopy of LkCa 3 was collected at the Harvard-Smithsonian Center for Astrophysics (CfA) over a period of a little more than nine years beginning in November of 1985. This is largely the same material used by Mathieu (1994) to obtain the preliminary single-lined orbit of the system, but the details are reported here for the first time. Observations were acquired with nearly identical echelle spectrographs (Digital Speedometers; Latham 1985, 1992) attached to the 1.5 m Tillinghast reflector at the F. L. Whipple Observatory on Mount Hopkins (AZ), and the 4.5 m-equivalent MMT also on Mount Hopkins, prior to its conversion to a monolithic 6.5 m telescope. A single echelle order 45 \AA wide was recorded using intensified photon-counting Reticon detectors, at a central wavelength of about 5190 \AA that includes the lines of the Mg I b triplet. The resolving power of these instruments was $\lambda/\Delta\lambda \approx 35,000$, and the signal-to-noise ratios of the observations range from 9 to 21 per resolution element of 8.5 km s^{-1} . A total of 58 exposures were obtained, although four were later discarded because of moonlight

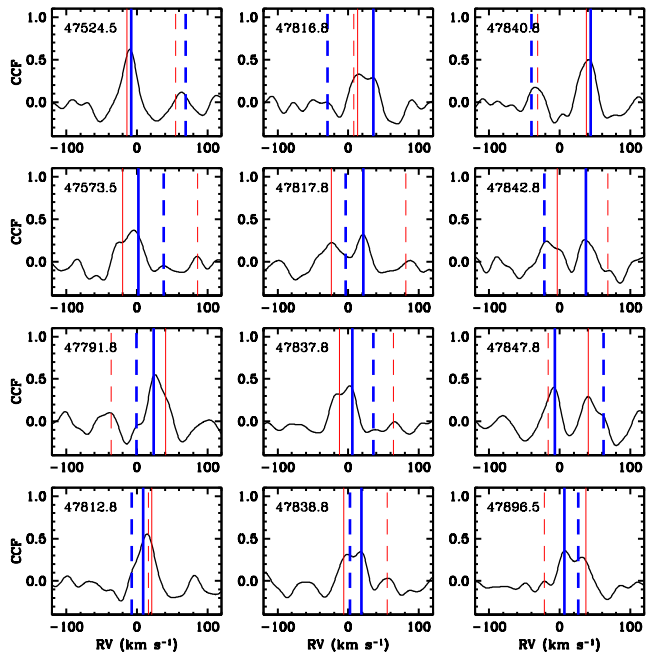


FIG. 1.— Sample one-dimensional cross-correlation functions for LkCa 3 from our optical CfA spectra, with the final RVs of the four components at the corresponding phases as measured with QUADCOR marked with vertical lines. Thicker lines (blue in the online color version) correspond to LkCa 3 A (solid for the primary, dashed for the secondary), and thin lines (red) are for LkCa 3 B. The Julian date of the observation (HJD $- 2,400,000$) is indicated in each panel. Individual spectra have signal-to-noise ratios too low to permit a clear visual identification of spectral lines from the different components, and are thus not shown.

contamination or other problems.

The standard, one-dimensional cross-correlation functions for these spectra clearly show a peak corresponding to the star reported by Mathieu (1994) to have a variable radial velocity (RV) with a period of 12.94 days. Occasionally, however, a second peak of similar height is also visible (see Figure 1). Shortly after the Mathieu (1994) publication the spectra of LkCa 3 were subjected to an analysis with TODCOR, a two-dimensional cross-correlation technique that had just been introduced by Zucker & Mazeh (1994). TODCOR is designed to measure radial velocities from double-lined spectra, and uses two templates, one for each set of lines. It was discovered that the velocities from the second set of lines were not changing with the same period as the first set, but varied instead with a shorter period of 4.06 days. Given that LkCa 3 is a near equal brightness visual binary with an angular separation ($\sim 0''.5$) that is smaller than the width of the spectrograph slit ($1''$), this immediately suggested the quadruple nature of the system, with each visual component being in turn a spectroscopic binary. We refer to the 12.94-day binary as system A, with components Aa and Ab, and to the stars in the other system as Ba and Bb, although from these observations alone we cannot identify which visual component is A and which is B.

This discovery languished for a time, and only more recently did we return to the system in an attempt to detect the secondary star of the 12.94-day system. For this we reanalyzed the spectra using TRICOR, an extension of TODCOR to three dimensions (Zucker et al. 1995). The effort was successful, and showed the faint

secondary to be only half as massive as the primary. A similar exercise with TRICOR resulted in the detection of the secondary of the 4.06-day binary, which also has about half the mass of its primary.

The TRICOR velocities obtained from these two analyses are likely biased to some extent due to line blending from the fourth star, whose presence is ignored in each case. With proof that the spectra are in fact quadruple-lined, we proceeded to reanalyze them one more time with QUADCOR, which is an extension of TODCOR to four dimensions (Torres et al. 2007). In previous studies of solar-type stars with similar spectroscopic material we have typically used synthetic spectra as templates for the cross-correlations, based on model atmospheres by R. L. Kurucz. Here, however, all components are M stars, and calculated spectra become less realistic at these low temperatures, particularly at high resolution. Instead, we used strong exposures of M stars obtained with the same instrumentation, covering a range of spectral types. We applied rotational broadening following the prescription of Gray (2005). A large number of template combinations was tried, guided initially by the results described below from the near-infrared spectra. In those observations the visual components are spatially resolved, so the spectra are only double-lined, making template selection easier. For the rotational broadening we were also guided by the results from Nguyen et al. (2012), described later in Sect. 3, who resolved some of the components spectroscopically with observations of much higher signal-to-noise ratio than ours.

For the 12.94-day binary, the templates that provided the best match to the observations, as measured by the cross-correlation value averaged over all exposures, are GJ 49 (M1.5; adopted $RV = -5.48 \text{ km s}^{-1}$) and GJ 699 (M4; $RV = -108.77 \text{ km s}^{-1}$), rotationally broadened to 12 km s^{-1} and 4 km s^{-1} , respectively. For the 4.06-day binary we used GJ 846 (M0; $RV = +18.61 \text{ km s}^{-1}$) and GJ 15 A (M2; $RV = +12.72 \text{ km s}^{-1}$), broadened to 16 km s^{-1} and 14 km s^{-1} . Our final QUADCOR velocities are presented in Table 1, along with the individual uncertainties. These are typically 1.7 and 5.7 km s^{-1} for stars Aa and Ab, and 2.6 and 11 km s^{-1} for stars Ba and Bb. To monitor the zero-point of our velocity system we obtained exposures of the dusk and dawn sky, and applied small run-to-run corrections as described by Latham (1992). These corrections are included in measurements listed in Table 1.

In addition to the radial velocities we determined the light ratios between the stars at the mean wavelength of our spectra (5190 \AA ; see Torres et al. 2007). The values, averaged over all exposures, are $\ell_{Ab}/\ell_{Aa} = 0.161 \pm 0.012$, $\ell_{Ba}/\ell_{Aa} = 0.938 \pm 0.042$, and $\ell_{Bb}/\ell_{Aa} = 0.223 \pm 0.018$. The fractional light contributions are thus 0.43 (Aa), 0.07 (Ab), 0.40 (Ba), and 0.10 (Bb). As a result the combined light of A is the same as that of B, at least at these wavelengths.

2.2. Near-infrared spectroscopy

Near-infrared spectra were obtained at the Keck II 10 m telescope (Mauna Kea, HI) using the facility, cross-dispersed cryogenic spectrograph NIRSPEC (McLean et al. 1998, 2000). NIRSPEC employs a 1024×1024 InSb array detector, which can accommodate

several high-resolution spectral orders simultaneously. We observed in the H band centered at $\sim 1.555 \mu\text{m}$, corresponding to NIRSPEC order 49. The advantage of this spectral region is that while it lacks significant contamination from telluric absorption lines, thus avoiding the need to divide by the spectrum of an early-type star, numerous OH night sky emission lines are distributed across the spectral range (Rousselot et al. 2000), supplying an excellent means of inherent wavelength and zero-point calibration. It is also rich in deep atomic and molecular lines found in G- through M-type stars. Spectra were recorded in sets of four exposures in an ‘ABBA’ dither pattern to allow for background subtraction and elimination of bad pixels. A two-pixel slit width yielded a spectral resolution of $\lambda/\Delta\lambda \approx 30,000$. In total, five observations were obtained in a period between 2003 and 2010 (Table 2).

On UT 2006 December 14 and 2010 December 12 we used NIRSPEC in high-angular resolution mode behind the Keck II adaptive optics (AO) system. This facilitated separation of the $\sim 0''.5$ pair, LkCa 3 A and B. Natural seeing conditions on these nights were $\sim 1''$ and $0''.5$, respectively. Because of multiple reflections in the complex AO light path, integration times per exposure were 300 s even for these relatively bright stars. The NIRSPEC slit is re-imaged behind the AO system by a factor of ~ 11 , making it prohibitively small for collecting light from OH night sky emission lines. Comparison lamp lines were thus recorded to accomplish the dispersion solution and set the zero-point.

On the other three nights (UT 2003 November 5, 2004 December 25, and 2010 November 22) we did not use AO. Although the seeing was relatively good ($0''.4$, $0''.3$, and $0''.6$, respectively) the point spread functions (PSFs) of the spectral traces overlapped in the two-dimensional spectra. With the higher throughput, shorter integration times of 60 to 120 s per exposure were adequate.

Spectra were extracted with the REDSPEC IDL package⁶, available on the Keck website and specifically designed for the analysis of NIRSPEC data. These procedures correct for spatial and spectral distortions in the two-dimensional spectra. Reduction of the AO data was trivial; the same procedure was followed as in, e.g., Rosero et al. (2011). However, to extract individual spectra from the overlapping PSFs in the non-AO data it was necessary to use REDSPEC to extract the rectified two-dimensional spectra and then apply further operations to separate LkCa 3 A and B. Customized IDL procedures were employed to determine the best Gaussian parameters for the A and B PSFs. The stellar signal for each of the 1024 columns in the cross-dispersion direction of the rectified two-dimensional spectrum was then fit with two overlapping model Gaussians, varying the heights to identify the flux (the Gaussian maximum) of each component individually. The reduced and barycenter-corrected spectra for order 49 are shown in Figures 2 and 3.

Since our procedures separate LkCa 3 A and B, the NIR spectra are only double-lined, and the velocity analysis is considerably simpler than in the optical. Furthermore, with previous knowledge of the orbits from our optical spectra, the NIR observations allow us to unambiguously

⁶ <http://www2.keck.hawaii.edu/inst/nirspec/redspec/index.html>

TABLE 1
HELIOCENTRIC RADIAL VELOCITIES FOR LkCa 3 FROM CFA

HJD (2,400,000+)	Phase (LkCa 3 A)	RV_{Aa} (km s^{-1})	σ_{Aa} (km s^{-1})	RV_{Ab} (km s^{-1})	σ_{Ab} (km s^{-1})	Phase (LkCa 3 B)	RV_{Ba} (km s^{-1})	σ_{Ba} (km s^{-1})	RV_{Bb} (km s^{-1})	σ_{Bb} (km s^{-1})
47524.6317	0.4974	-7.98	1.66	69.23	6.51	0.4221	-13.76	2.67	55.05	11.84
47543.6560	0.9674	46.80	1.85	-46.59	7.23	0.0991	44.02	2.96	-32.18	13.15
47544.5958	0.0400	41.91	1.82	-46.16	7.11	0.3302	-6.40	2.91	55.87	12.94
47545.5693	0.1152	30.84	1.98	-8.94	7.76	0.5695	-18.93	3.18	75.34	14.13
47555.6846	0.8968	37.86	1.85	-38.64	7.23	0.0563	47.38	2.96	-59.42	13.15
47573.6815	0.2874	1.97	2.06	37.78	8.08	0.4807	-20.05	3.31	86.39	14.70
47791.8706	0.1466	23.83	1.60	-0.48	6.26	0.1213	40.60	2.56	-36.38	11.39
47810.9024	0.6171	-2.93	2.06	47.35	8.08	0.8002	28.11	3.31	19.40	14.70
47811.9441	0.6976	7.41	1.98	34.83	7.76	0.0563	49.65	3.18	-63.19	14.13
47816.8581	0.0773	35.64	1.82	-29.37	7.11	0.2643	13.35	2.91	7.77	12.94
47817.8777	0.1561	21.58	1.91	-3.51	7.48	0.5150	-23.91	3.06	81.84	13.61
47818.7831	0.2260	13.75	1.85	30.64	7.23	0.7376	11.54	2.96	5.53	13.15
47822.7730	0.5343	-7.55	1.62	55.88	6.34	0.7185	14.18	2.60	6.91	11.54
47837.7335	0.6903	5.99	1.85	35.93	7.23	0.3964	-12.60	2.96	64.12	13.15
47838.7451	0.7685	18.77	1.66	2.40	6.51	0.6451	-6.36	2.67	55.15	11.84
47839.7495	0.8461	35.90	1.85	-13.02	7.23	0.8921	36.47	2.96	-29.94	13.15
47840.7298	0.9218	44.13	2.02	-39.68	7.92	0.1331	37.99	3.24	-31.38	14.41
47842.7792	0.0802	37.31	1.88	-21.38	7.35	0.6369	-3.40	3.01	68.21	13.38
47845.7562	0.3102	3.17	1.40	50.46	5.49	0.3688	-7.08	2.25	61.82	9.99
47846.8502	0.3947	-7.85	1.79	55.85	7.00	0.6377	-7.78	2.87	66.30	12.73
47847.8078	0.4687	-6.86	1.79	62.22	7.00	0.8732	40.86	2.87	-16.04	12.73
47868.8798	0.0969	34.59	2.45	-17.70	9.60	0.0536	46.14	3.93	-72.48	17.47
47869.7600	0.1650	22.56	1.34	13.18	5.24	0.2700	8.14	2.15	1.26	9.54
47870.8110	0.2462	5.48	1.12	20.35	4.40	0.5284	-19.69	1.80	98.67	8.00
47871.7089	0.3155	-4.41	1.39	43.28	5.44	0.7491	14.47	2.23	6.69	9.90
47873.7834	0.4758	-9.62	1.71	60.79	6.69	0.2591	11.34	2.74	4.99	12.18
47878.7773	0.8617	36.01	1.49	-12.20	5.84	0.4868	-26.55	2.39	86.12	10.62
47896.5666	0.2363	6.64	1.58	26.22	6.18	0.8602	37.41	2.53	-21.89	11.25
47897.5831	0.3148	-0.39	1.60	50.57	6.26	0.1101	42.12	2.56	-34.62	11.39
47898.5768	0.3916	-4.76	1.56	49.87	6.11	0.3544	-6.53	2.50	63.72	11.12
47900.5812	0.5465	-5.66	1.56	55.83	6.11	0.8472	36.94	2.50	-28.18	11.12
47901.5750	0.6233	-2.31	1.62	46.30	6.34	0.0915	45.42	2.60	-43.68	11.54
47902.6324	0.7050	9.49	1.64	13.53	6.42	0.3515	-7.67	2.63	59.96	11.69
47903.6486	0.7835	20.08	1.52	-3.59	5.97	0.6013	-15.97	2.44	58.75	10.86
47904.6876	0.8638	35.19	1.51	-17.34	5.90	0.8567	38.25	2.42	-32.03	10.74
47905.7074	0.9426	44.86	1.56	-43.52	6.11	0.1075	41.80	2.50	-36.67	11.12
47906.7332	0.0218	46.15	1.52	-45.76	5.97	0.3596	-9.23	2.44	51.82	10.86
47908.8453	0.1850	18.71	1.88	13.93	7.35	0.8789	39.42	3.01	-30.94	13.38
47958.6627	0.0343	43.85	1.51	-37.93	5.90	0.1262	39.91	2.42	-39.07	10.74
47960.6862	0.1907	14.65	1.54	17.75	6.04	0.6237	-8.38	2.47	67.04	10.99
47965.6562	0.5747	-5.97	1.52	51.71	5.97	0.8455	36.34	2.44	-34.40	10.86
47994.6117	0.8121	23.37	1.66	-0.56	6.51	0.9641	40.93	2.67	-45.64	11.84
47995.6062	0.8889	40.56	2.21	-39.45	8.64	0.2086	30.21	3.54	-17.69	15.72
47996.6027	0.9659	45.75	1.91	-49.83	7.48	0.4536	-19.22	3.06	101.16	13.61
48167.9722	0.2074	12.62	1.56	23.07	6.11	0.5838	-16.34	2.50	58.90	11.12
48175.9425	0.8233	27.87	1.07	-9.54	4.17	0.5433	-22.26	1.71	85.27	7.59
48194.7904	0.2796	4.58	1.23	43.45	4.80	0.1769	30.45	1.97	-9.18	8.74
48195.7994	0.3576	-3.94	1.26	52.34	4.95	0.4250	-14.42	2.03	68.47	9.00
48200.8740	0.7497	13.47	1.51	18.43	5.90	0.6725	-1.12	2.42	68.04	10.74
48201.8223	0.8230	28.73	1.71	-17.04	6.69	0.9057	42.57	2.74	-35.80	12.18
48291.7312	0.7701	18.87	1.46	7.43	5.71	0.0093	49.69	2.34	-72.09	10.40
48943.8887	0.1614	19.25	1.68	2.27	6.60	0.3386	-7.05	2.70	60.77	12.01
49268.9754	0.2804	0.85	1.85	51.55	7.23	0.2594	17.34	2.96	10.57	13.15
49705.7008	0.0256	41.91	1.68	-50.84	6.60	0.6260	-10.34	2.70	55.63	12.01

TABLE 2
HELIOCENTRIC RADIAL VELOCITIES FOR LkCa 3 IN THE NEAR INFRARED

HJD (2,400,000+)	Phase (LkCa 3 A)	RV_{Aa} (km s^{-1})	σ_{Aa} (km s^{-1})	RV_{Ab} (km s^{-1})	σ_{Ab} (km s^{-1})	Phase (LkCa 3 B)	RV_{Ba} (km s^{-1})	σ_{Ba} (km s^{-1})	RV_{Bb} (km s^{-1})	σ_{Bb} (km s^{-1})
52949.0510	0.6347	-0.94	0.70	40.52	1.10	0.9858	47.79	1.50	-54.81	2.30
53364.7389	0.7544	15.55	0.70	10.78	1.10	0.1804	27.35	1.50	-16.42	2.30
54083.9544	0.3272	-3.14	0.70	46.05	1.10	0.9956	48.67	1.50	-54.49	2.30
55523.0858	0.5269	-6.78	0.70	52.86	1.10	0.7982	19.09	1.50	-9.52	2.30
55542.7560	0.0467	40.81	0.70	-41.28	1.10	0.6340	-9.45	1.50	55.44	2.30

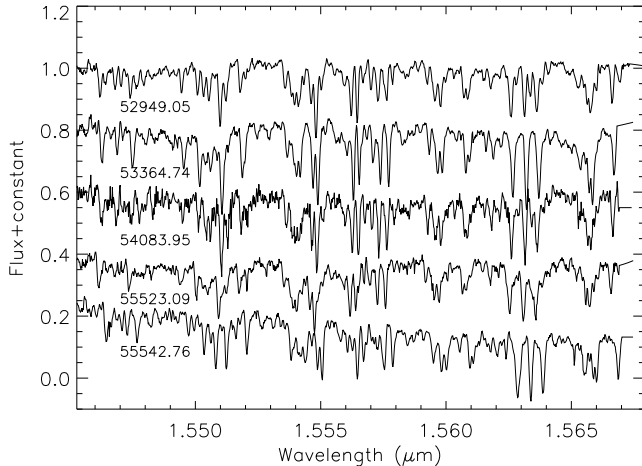


FIG. 2.— Five epochs of NIR Keck spectra for LkCa 3 A (West) in NIRSPEC order 49, with barycentric corrections applied; Julian dates of the observations (HJD–2,400,000) are indicated. The spectra have been normalized to unity and an arbitrary additive constant used to offset the spectra for display.

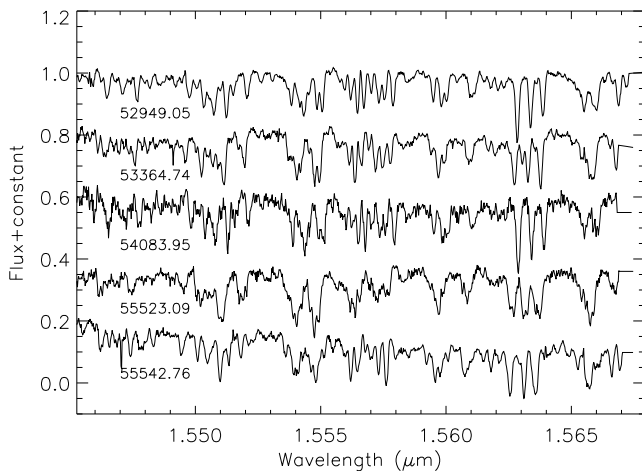


FIG. 3.— Same as Figure 2, for LkCa 3 B (East).

identify star A ($P = 12.94$ days) as the Western component, and star B ($P = 4.06$ days) as the Eastern one.

Radial velocities were measured using the TODCOR algorithm of Zucker & Mazeh (1994). As with our optical spectra, we correlated each of our observations against a grid of observed template spectra of high signal-to-noise ratio (Prato et al. 2002a) seeking the highest correlation coefficient averaged over all exposures. These IR template spectra were rotationally broadened by convolving them with the line-broadening function of Gray (2005). For LkCa 3 A the best fit was produced combining the M2 star GJ 752 A (adopted $RV = +34.2 \text{ km s}^{-1}$) rotationally broadened to 12 km s^{-1} with the M4 star GJ 402 ($RV = -3.1 \text{ km s}^{-1}$) spun up to 6 km s^{-1} , as the primary and secondary templates, respectively. For LkCa 3 B the best templates were 61 Cyg B (K7; $RV = -65.4 \text{ km s}^{-1}$) and GJ 436 (M2.5; $RV = +7.8 \text{ km s}^{-1}$), rotated to 18 and 14 km s^{-1} , respectively. The nominal spectral types of these templates are within one sub-type of the templates adopted in the optical for the same components, and the rotational velocities are also quite similar (within 2 km s^{-1}). Average values for the latter are reported later in Sect. 4.

The flux ratios in the H band were found to be 0.47 ± 0.06 for LkCa 3 A (ratio Ab/Aa), and 0.52 ± 0.08 for LkCa 3 B (Bb/Ba), which are averages over the 5 observations in each case. The NIR radial velocities in the heliocentric frame are presented in Table 2, along with their estimated uncertainties.

2.3. High-resolution imaging

We observed LkCa 3 on UT 2008 January 17 with the adaptive optics system at the W. M. Keck Observatory, using the near-infrared camera NIRC2 (Wizinowich et al. 2000). A series of 10 dithered images were collected in the narrow-band H and K continuum regions, using a 5-point dither pattern with an offset of $2''$. Each image consisted of 10 co-added 0.5 s exposures. The images were flat-fielded using dark-subtracted, medianed dome flats. Pairs of dithered images were subtracted to remove the sky background.

We used the brighter, Western component (LkCa 3 A) as a PSF reference to measure the relative separation and flux ratio of the Eastern component relative to the Western one. We corrected the positions for geometric distortions in the detector, used a plate scale of $9.952 \pm 0.001 \text{ mas pixel}^{-1}$, and subtracted $0^{\circ}.252 \pm 0^{\circ}.009$ from the raw position angles to correct for errors in the orientation of the camera relative to the true North (Yelda et al. 2010). Taking the average of the H - and K -band images, we measured an angular separation of $483.73 \pm 0.28 \text{ mas}$ and a position angle of $69^{\circ}.068 \pm 0^{\circ}.035$ East of North, at Julian date 2,454,482.872. We also determined the flux ratio of the Eastern relative to Western component to be 0.942 ± 0.011 at H , and 0.9404 ± 0.0074 at K . Uncertainties were derived by analyzing multiple images individually and computing the standard deviation.

While the angular separation between the visual components of LkCa 3 has remained the same since its discovery by Leinert et al. (1993), the position angle has decreased significantly by almost 10° . This could be a sign of orbital motion, but it may also be the result of a small difference in proper motion between two unbound members of the star-forming region. Our spectroscopic orbital solutions described in the next section indicate that the center-of-mass velocities of LkCa 3 A and B are very close to each other (within 0.4 km s^{-1}), but this, too, is consistent with either scenario. Though the current observations are insufficient to confirm the physical association, an estimate of the likelihood of a chance alignment in Taurus strongly favors the binary hypothesis. Based on the stellar densities near LkCa 3 reported by Gómez et al. (1993), we compute a probability of finding two unbound stars within only $0''.5$ of each other to be $\sim 10^{-7}$, and for the remainder of the paper we will assume that LkCa 3 A and B are physically bound. At the distance to the object of 133 pc estimated below in Sect. 5.1, the projected linear separation of the visual binary is approximately 64 AU , and the orbital period roughly 400 yr .

3. SPECTROSCOPIC ORBITAL SOLUTIONS

The optical and near-infrared RVs were used simultaneously to compute weighted orbital solutions for each of the two binaries. A velocity offset for the NIR data (in the sense CfA minus Keck) was added as a free parameter to take into account possible differences in the

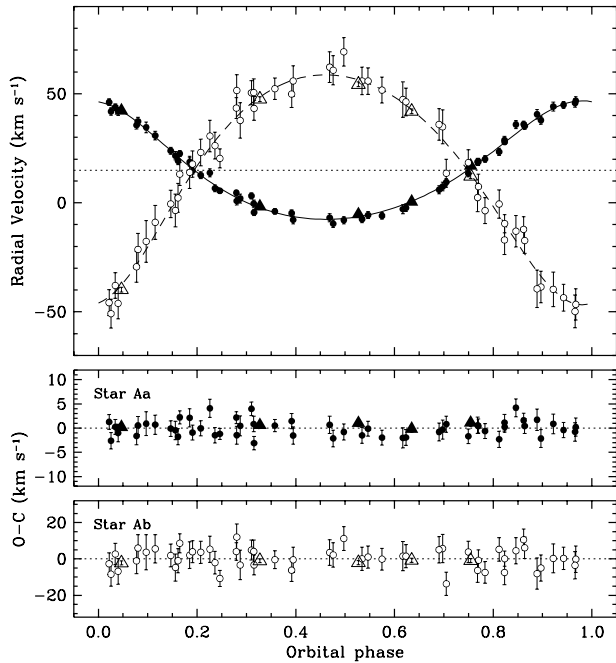


FIG. 4.— Radial-velocity measurements for LkCa 3 A (West) along with our weighted orbital fit. Filled symbols are for star Aa (circles for the CfA observations, triangles for the NIR measurements), and open symbols for star Ab. The dotted line in the top panel represents the center-of-mass velocity of the binary, and phase 0.0 corresponds to periastron passage. Residuals are shown at the bottom.

zero points. We found these offsets to be significant for both binaries. The resulting orbital elements and other derived quantities are listed in Table 3. While the eccentricity of the LkCa 3 A orbit is clearly non-zero, that of LkCa 3 B in our initial solution was very small ($e = 0.025 \pm 0.011$), and statistically insignificant according to the test of Lucy & Sweeney (1971), with a false alarm probability of 0.08. We therefore chose to adopt here the parameters from a solution for a circular orbit. As noted earlier, the velocities of the centers of mass, γ , are essentially the same for the two binaries (Table 3). Graphical representations of the observations and final orbit models are shown in Figure 4 and Figure 5. The NIR velocities in these figures have been corrected for the offsets mentioned above.

In a recent study by Nguyen et al. (2012), a handful of radial-velocity measurements were reported for LkCa 3 in the context of a spectroscopic multiplicity survey in Chamaeleon and Taurus-Auriga. The authors measured three of the components at each of four epochs, but without full knowledge of the complexity of the system they were unable to provide a consistent explanation of the observed RV changes at the time. Our spectroscopic orbits now permit us to ascertain that their ‘star 1’ is the one we refer to as Aa, while their stars 2 and 3 are generally Ba and Bb, respectively, but occasionally another component or a blend.

4. PHYSICAL PROPERTIES

Under the working assumption that the four stars in LkCa 3 are coeval, our estimates of the flux ratios along with other constraints may be used with a set of PMS evolutionary models to infer the age of the system, as well as its distance, D . The minimum masses from our

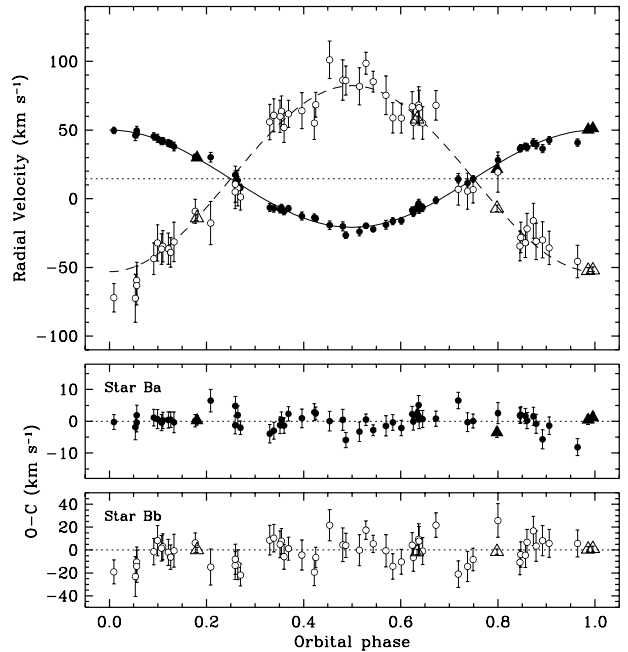


FIG. 5.— Same as Figure 4 for LkCa 3 B (East). The orbit is assumed to be circular. Phase 0.0 corresponds to the phase of maximum primary velocity.

spectroscopic orbits additionally allow us derive the inclination angles of the two binaries, i_A and i_B . We describe this in the next section. The observables we incorporate, aside from the minimum masses, are listed in Table 4, and include $V(RI)_C JHK_s$ apparent magnitudes from the literature, flux ratios measured here in the H and K bands as well as in V (converted from 5190 \AA), and estimates of the effective temperatures of the four stars. A comparison of our LkCa 3 B/A flux ratios from Sect. 2.3 with similar measurements from the literature indicates significant variability in H and K , which is not unexpected for young and active stars such as these. For this reason we have used a weighted average of all available B/A estimates, rather than our own single-epoch measurement. The flux ratios in V and H measured between individual stars are already averages of several epochs from our optical and NIR spectroscopy.

In order to obtain the effective temperatures we made the assumption that each component of LkCa 3 is adequately represented by the M stars adopted as templates, both in the optical QUADCOR analysis and in the near-infrared TODCOR analyses. Since each component used a different template in the optical than in the NIR (see Sect. 2.1 and Sect. 2.2), two estimates of T_{eff} may be obtained for each of the four stars Aa, Ab, Ba, and Bb. A common practice in the field of PMS stars is to assign temperatures directly from spectral types using a look-up table, of which there are many. Here we have taken a more quantitative approach independent of the spectral type labels. When available, we adopted temperature estimates for the eight template stars derived from NIR spectroscopy performed by Rojas-Ayala et al. (2012). This was the case for GJ 402, GJ 699, 61 Cyg B, GJ 436, and GJ 15 A. In other cases we made our own T_{eff} estimates from optical and NIR colors in the literature along with the recent color/temperature calibrations of Boyajian et al. (2012). This procedure was used

TABLE 3
SPECTROSCOPIC ORBITAL SOLUTIONS FOR LKCa 3.

Parameter	LkCa 3 A (West)	LkCa 3 B (East)
Adjusted quantities		
P (days)	12.941865 ± 0.000075	4.0676115 ± 0.0000085
γ (km s^{-1}) ^a	$+14.97 \pm 0.22$	$+14.59 \pm 0.35$
ΔRV (km s^{-1}) ^b	$+1.46 \pm 0.35$	$+2.52 \pm 0.71$
K_a (km s^{-1})	27.16 ± 0.31	35.37 ± 0.45
K_b (km s^{-1})	52.75 ± 0.77	67.7 ± 1.2
e	0.1735 ± 0.0090	0 (fixed)
ω_a (deg)	10.2 ± 2.7	...
T (HJD - 2,400,000) ^c	$48,501.777 \pm 0.094$	$48,499.1416 \pm 0.0080$
Derived quantities		
$M_a \sin^3 i$ (M_\odot)	0.432 ± 0.015	0.303 ± 0.013
$M_b \sin^3 i$ (M_\odot)	0.2221 ± 0.0062	0.1585 ± 0.0050
$q \equiv M_b/M_a$	0.5148 ± 0.0085	0.522 ± 0.012
$a_a \sin i$ (10^6 km)	4.760 ± 0.052	1.979 ± 0.025
$a_b \sin i$ (10^6 km)	9.25 ± 0.13	3.788 ± 0.069
$a \sin i$ (R_\odot)	20.13 ± 0.21	8.29 ± 0.10
Other quantities pertaining to the fit		
N_{obs} (CfA / Keck)	54 / 5	54 / 5
Time span (yr)	21.95	21.95
σ_{RV} for CfA (km s^{-1})	1.71 / 5.75	2.64 / 11.48
σ_{RV} for Keck (km s^{-1})	0.76 / 1.56	1.97 / 1.18

^a Formal uncertainties exclude any errors in the absolute RVs of the cross-correlation templates.

^b Velocity offset in the sense (CfA–Keck).

^c For LkCa 3 A the time listed corresponds to periastron passage; for LkCa 3 B it is the time of maximum primary velocity. In both cases the epoch is the one nearest to the average time of observation, to minimize the uncertainty.

for GJ 752 A, GJ 49, and GJ 846. For the photometric temperature determinations we require also an estimate of the reddening, which we obtained from four different sources as listed in Table 4. The adopted average with a conservative uncertainty is $E(B - V) = 0.10 \pm 0.05$, which is in line with other estimates for the region. Extinction corrections for each passband were applied following Cardelli et al. (1989). Finally, we averaged the temperatures for the optical and NIR templates used for each component of LkCa 3; these mean values are reported also in Table 4.

5. COMPARISON WITH STELLAR EVOLUTION MODELS

The collection of observational constraints listed in Table 4, along with the minimum masses from Table 3, were compared in a χ^2 sense with PMS isochrones for solar metallicity from the Dartmouth series (Dotter et al. 2008). Specifically, we explored a large number of combinations of ages, distances D , and orbital inclination angles i_A and i_B over wide ranges of these variables and in small steps. For each trial set of inclination angles and age we computed the absolute masses of the four stars using our spectroscopic minimum masses. We also read off their temperatures from the corresponding isochrone, for comparison with our measured T_{eff} values, as well as their brightness in the relevant bandpasses, from which the flux ratios can be computed. Finally, with the trial distance and the adopted reddening we predicted the apparent magnitudes needed to compare with the values in Table 4.

We applied a simple grid search procedure to find the set of four variables that yields the best overall fit (lowest χ^2), and arrived at a satisfactory solution for a distance of $D = 127_{-13}^{+16}$ pc, an age of $1.6_{-0.5}^{+0.9}$ Myr, and best-fit in-

clination angles for the two binary orbits of $i_A = 70.0_{-4.5}^{+5.5}$ deg and $i_B = 57.0_{-2.5}^{+3.0}$ deg. The 1- σ uncertainties were derived by perturbing all observables in a Monte Carlo fashion assuming they are normally distributed, repeating the isochrone fitting 1000 times, and computing the 15.85 and 84.13 percentiles of the resulting distributions. The observations and best-fit 1.6-Myr isochrone are displayed in a diagram of absolute visual magnitude versus T_{eff} in the top panel of Figure 6, along with evolutionary tracks from the same models. The dispersion around the 1.6-Myr isochrone in this plane is due mostly to errors in the effective temperatures. Indeed, the lower panel of the figure shows that the scatter is significantly reduced when plotting $V - H$ instead of T_{eff} , which we are able to do because this color index can be measured individually for all four stars from the information given in Table 4. The temperature errors may arise in part from the limited selection of templates we have, both in the optical and in the NIR, from uncertainties in the calibrations involved in the T_{eff} determinations, and from differences in surface gravity between dwarfs and PMS stars (see, e.g., Luhman 1999).

Our age estimate for LkCa 3 is consistent with other estimates of a few Myr for T Tauri stars in Taurus-Auriga (e.g., Kenyon & Hartmann 1995; Luhman & Reike 1998; Palla & Stahler 2002; Briceño et al. 2002), but is of course model-dependent. Similarly, our distance estimate agrees with the canonical value for the region of 140 pc. LkCa 3 is projected onto the general area of the Lynds 1495 molecular cloud at the Western edge of the Taurus-Auriga star-forming region. Very precise trigonometric parallax measurements with the Very Long Baseline Array (VLBA) have shown that different areas within the complex are at slightly different distances. In

TABLE 4
OBSERVATIONAL CONSTRAINTS FOR LKCA 3 FOR
COMPARISON WITH STELLAR EVOLUTION MODELS.

Parameter	Value	Source
V (mag)	12.09 ± 0.03	1
R_C (mag)	11.05 ± 0.04	1
I_C (mag)	9.79 ± 0.04	1
J (mag)	8.363 ± 0.032	2
H (mag)	7.625 ± 0.023	2
K_s (mag)	7.423 ± 0.021	2
Ab/Aa V -band flux ratio	0.154 ± 0.012	3
Ba/Aa V -band flux ratio	0.989 ± 0.044	3
Bb/Aa V -band flux ratio	0.232 ± 0.019	3
Ab/Aa H -band flux ratio	0.47 ± 0.06	4
Bb/Ba H -band flux ratio	0.52 ± 0.08	4
B/A H -band flux ratio	0.878 ± 0.079	5
B/A K -band flux ratio	0.891 ± 0.048	5
Adopted $E(B - V)$ (mag)	0.10 ± 0.05	6
T_{eff} of Aa (K)	3570 ± 100	7
T_{eff} of Ab (K)	3290 ± 100	7
T_{eff} of Ba (K)	3870 ± 150	7
T_{eff} of Bb (K)	3490 ± 150	7
$v \sin i$ of Aa (km s^{-1})	12 ± 2	8
$v \sin i$ of Ab (km s^{-1})	5 ± 4	8
$v \sin i$ of Ba (km s^{-1})	17 ± 1	8
$v \sin i$ of Bb (km s^{-1})	14 ± 1	8
P_{rot} of star Aa (days)	7.38 ± 0.40	9
P_{rot} of star Ba (days)	4.06 ± 0.13	9

NOTE. — Sources are: 1. Kenyon & Hartmann (1995); 2. 2MASS (Cutri et al. 2003); 3. Measured from our optical spectra (mean wavelength of 5190 \AA) and converted to the V band; 4. Measured from our NIR spectra; 5. Weighted average of one measurement from this work (Sect. 2.3) and several others (two in H and five in K) from Leinert et al. (1993), Ghez et al. (1993), Woitas et al. (2001a), Woitas et al. (2001b), White & Ghez (2001), and McCabe et al. (2006); 6. Average of estimates based on the dust maps from Hakkila et al. (1997), Schlegel et al. (1998), Drimmel et al. (2003), and Amôres & Lépine (2005); 7. Estimates derived here based on spectroscopic determinations for the template stars from Rojas-Ayala et al. (2012) or based on color/temperature calibrations by Boyajian et al. (2012); 8. Average of determinations based on our optical and NIR spectra, with conservative uncertainties; 9. Measured here using the photometric observations of Norton et al. (2007) (see text).

particular, PMS stars near Lynds 1495 including Hubble 4, HDE 283572, and V773 Tau (which happens to also be a quadruple system and is only $20'$ away from LkCa 3) have an average distance of about 130 pc (Torres et al. 2007, 2012), whereas stars on the Eastern side of the complex (T Tau N and HP Tau/G2; Loinard et al. 2007; Torres et al. 2009) tend to have larger VLBA distances of 147–160 pc. Our estimate of 127^{+16}_{-13} pc for LkCa 3 is formally more consistent with the lower values than the higher ones. There are also differences in the proper motions of these two groups, and in their radial velocities, with the stars near Lynds 1495 having a lower mean RV around $+15 \text{ km s}^{-1}$ compared to $+18$ or $+19 \text{ km s}^{-1}$ for the far side of the complex. The average RV for LkCa 3 is $+14.8 \text{ km s}^{-1}$ (see Table 3), and its proper motion is also more similar to those of Hubble 4, HDE 283572, and V773 Tau than to those of T Tau N or HP Tau/G2. Thus, both the kinematic and distance evidence suggest that LkCa 3 is on the near side of the Taurus-Auriga complex.

The best fit to the Dartmouth models indicates the two

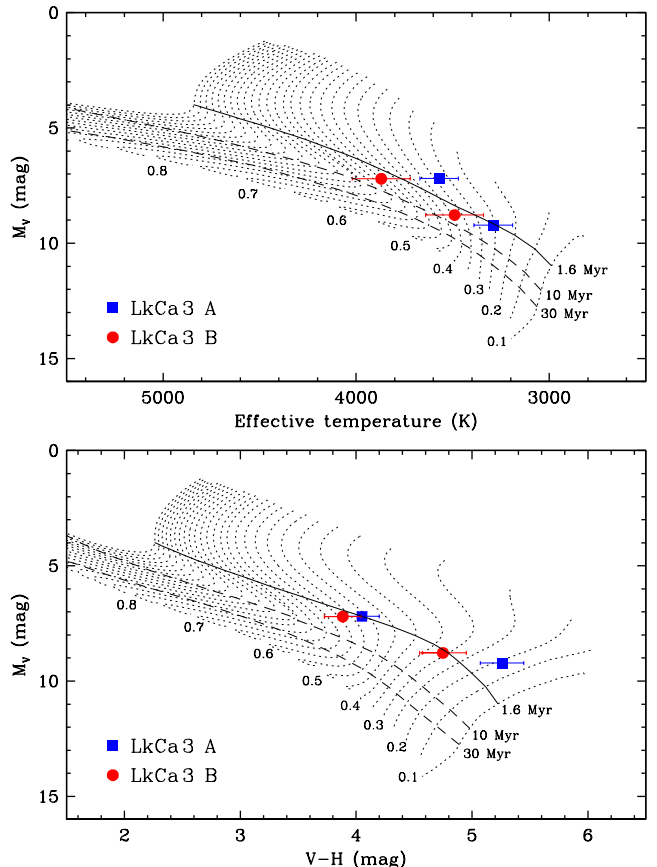


FIG. 6.— Observations for the four stars in LkCa 3 compared against PMS stellar evolution models from the Dartmouth series by Dotter et al. (2008). The best-fit 1.6-Myr isochrone is shown with a solid line (see text). Evolutionary tracks represented with dotted lines are labeled with their mass, in solar units; *Top*: Diagram of absolute visual magnitude versus effective temperature; *Bottom*: Same as above, illustrating the smaller scatter that results when using the $V - H$ color instead of T_{eff} .

binaries are nearly identical in their physical properties. The orbital inclination angles i_A and i_B combined with our minimum masses result in absolute masses for both primary stars (Aa and Ba) of about $0.51 M_{\odot}$, and masses for the secondaries (Ab and Bb) that are both about $0.27 M_{\odot}$. The radii predicted from the best-fit isochrone for these masses are approximately $1.56 R_{\odot}$ for the primaries and $1.22 R_{\odot}$ for the secondaries. The similarity between the properties of LkCa 3 A and B is consistent with their near-equal brightness, as reported earlier in Sect. 2.1 and Sect. 2.3. At face value the measurements in Table 4 suggest star A is slightly brighter than B in the H band ($\Delta H_{B-A} = +0.14 \pm 0.10$), but fainter in V ($\Delta V_{B-A} = -0.061 \pm 0.044$)⁷. While these differences may perhaps be real, and would be explained by the fact that the flux of each visual component is the sum of the contributions of two young stars, their significance is marginal.

5.1. Rotation as an additional constraint on models

The orbital periods of LkCa 3 A (12.94 days) and LkCa 3 B (4.06 days) are on either side of the observed tidal circularization period for PMS stars (considered as

⁷ These estimates are averages over time, though not necessarily over the same time interval for the different passbands.

a more or less coeval population of young objects), which represents the transition between circular and eccentric orbits (Mathieu et al. 1992; Mazeh 2008). This transition period is currently believed to be near 7.6 days, and is marked by the binary system RX J1603.9–3938, which has the longest-period circular orbit among bona-fide PMS stars (Melo et al. 2001; Covino et al. 2001). Our finding that the orbit of LkCa 3 B is essentially circular is consistent with this picture. Two other effects of tidal forces, the alignment of the spin axes with the orbital axis and the synchronization of the stellar rotations with the mean orbital motion, are predicted to occur much earlier than circularization (e.g., Hut 1981), so we may reasonably assume that these conditions also apply to the two components of LkCa 3 B. In other words, $i_{\text{rot}} = i_{\text{orb}}$ and $P_{\text{rot}} = P_{\text{orb}}$. If that is the case, then our measurement of the projected rotational velocities (which are strictly $v \sin i_{\text{rot}}$) provides a way to infer the mean stellar densities, as described by Torres et al. (2002), if we assume solid-body rotation. From the orbital elements and $v \sin i$ the density ρ of star Ba in solar units may be expressed as

$$\log \rho_{\text{Ba}} = -1.8724 - 2 \log P_{\text{orb}} + 2 \log(K_{\text{Ba}} + K_{\text{Bb}}) + \log K_{\text{Bb}} - 3 \log(v_{\text{Ba}} \sin i) \quad (1)$$

where P_{orb} is in days, the velocity semi-amplitudes K_{Ba} and K_{Bb} are in km s^{-1} , and the numerical constant is an update of that of Torres et al. (2002). A similar expression holds for $\log \rho_{\text{Bb}}$.

The non-circular orbit we find for LkCa 3 A (with $e = 0.1735 \pm 0.0090$) is consistent with the fact that its period is longer than the transition period for PMS stars. Rotational synchronization is therefore not guaranteed, so we can not assume that $P_{\text{rot}} = P_{\text{orb}}$. We note, however, that long-term photometric monitoring of LkCa 3 has shown a clear periodic signal with an amplitude of one or two tenths of a magnitude attributed to rotational modulation due to spots, although the multiplicity of the system has previously made it difficult to attribute the signal to any particular component. The period reported by Bouvier et al. (1995) from a 45-day observing campaign is 7.2 ± 0.6 days, and a similar result of 7.38 days was obtained by Norton et al. (2007) over a two-month period. More extensive observations by Grankin et al. (2008) between 1992 and 1998 yielded rotation periods in close agreement for each of 5 separate seasons having sufficient observations, with an average of 7.35 days. More recently Xiao et al. (2012) reported a period of 3.689 days from observations carried out over two months. This is very nearly half of the previous values, suggesting it may be a harmonic of the true period.

The rotation signal in LkCa 3 is likely to be due to either star Aa or Ba, simply on the basis that they are much brighter than the secondaries. We proceed under this assumption, and return to it below. Furthermore, if our earlier hypothesis of synchronized rotation for Ba and Bb is correct, then the signal would be associated with star Aa, which is also marginally the brighter. Evidence supporting this comes from the intensive photometric observations by Norton et al. (2007), totaling about 1350 measurements over a two-month period in a broad pass-band similar to $V+R$. Their power spectrum of the observations shows a hint of a second peak near a period

of 4 days. Our reanalysis of those data is illustrated in Figure 7. The top panel presents a Lomb-Scargle periodogram of the original observations with the 7.38-day signal clearly visible. The photometric amplitude of this signal is approximately 0.10 mag, and we estimate the uncertainty in the period to be 0.40 days. The peaks at periods under two days are all aliases with the 1-day cycle of the observations. This is seen more clearly in the second panel, where we have subjected the same data to the CLEAN algorithm of Roberts et al. (1987) that reduces the impact of the window function. We then subtracted a sine curve with a period of 7.38 days from the original measurements, and computed a Lomb-Scargle periodogram of the residuals (Figure 7c). A prominent peak is revealed at a period of 4.06 ± 0.13 days, with a false alarm probability smaller than 10^{-3} , determined from Monte Carlo simulations. This signal has a smaller photometric amplitude of about 0.05 mag. Once again the peaks at much shorter periods are aliases, as shown by the CLEANed power spectrum in the bottom panel of the figure. The close similarity with the orbital period of LkCa 3 B ($P_{\text{orb}} = 4.0676115$; Table 3) strongly suggests that this second signal corresponds to the rotational signature of star Ba, tidally locked to the mean orbital motion, as we had assumed. We conclude that the 7.38-day signal corresponds indeed to star Aa, which is then spinning more rapidly than the expected pseudo-synchronous rate ($P_{\text{pseudo}} = 11.0$ days; Hut 1981), and also faster than the periastron rate (9.0 days).

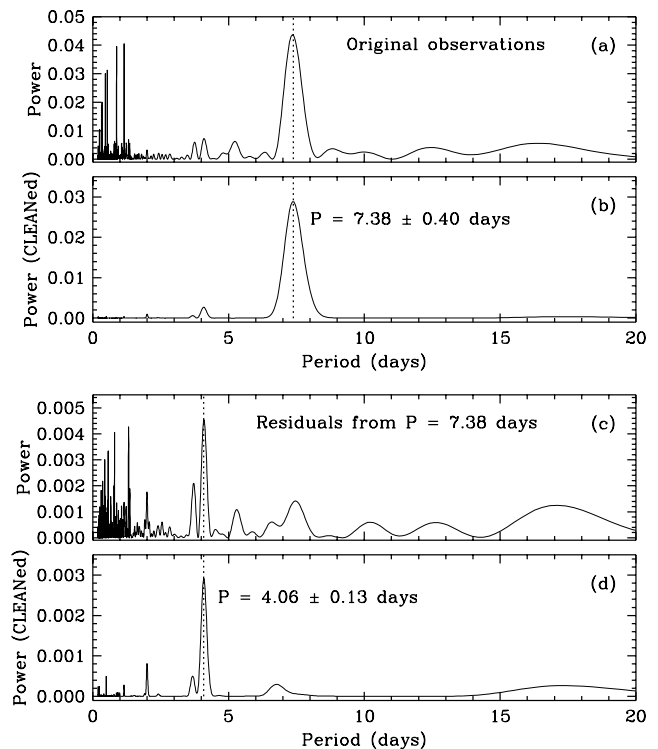


FIG. 7.— (a) Lomb-Scargle periodogram of the photometric observations of LkCa 3 by Norton et al. (2007); (b) Same as above, processed with the CLEAN algorithm of Roberts et al. (1987), and showing the 7.38-day rotational signal from star Aa; (c) Lomb-Scargle periodogram of the residuals from the Norton et al. (2007) data, after subtracting a sine-curve fit to remove the 7.38-day signal; (d) CLEANed power spectrum of the same residuals, revealing the highly significant 4.06-day signal that we attribute to star Ba.

The evidence that the above signals originate on the primaries of LkCa3 A and B rather than the secondaries relies on statistics from variability studies of non-accreting periodic T Tauri stars. If star Ab were the source of the 7.38-day signal, the photometric amplitude corrected for the light contribution of the other components of the quadruple system (Table 4) would be in excess of 1.5 mag. This is a very rare occurrence among WTTS (typical amplitudes are about 0.1–0.2 mag; see, e.g., Stassun et al. 1999; Grankin et al. 2008). On the other hand, if attributed to star Aa, the intrinsic amplitude would be only 0.24 mag, which is fairly common. Similarly for the 4.06-day signal, the intrinsic amplitudes we would infer for stars Ba and Bb are 0.5 mag and 0.12 mag. Though not unprecedented, the larger value is seen much less frequently than the smaller one in photometric studies of young stars. In any event, assignment of the observed signal to the primary or secondary in this case is less important, as rotational synchronization is likely to occur in both components given the short period and circular orbit, as discussed earlier.

With our measurement of the projected rotational velocity of Aa from Table 4 and knowledge of its rotation period, we may compute its mean density in a similar way as done for LkCa3 B with a slight modification of eq.(1):

$$\begin{aligned} \log \rho_{Aa} = & -1.8724 + \log P_{\text{orb}} - 3 \log P_{\text{rot}} + \\ & 2 \log(K_{Aa} + K_{Ab}) + \log K_{Ab} - \\ & 3 \log(v_{Aa} \sin i) + 1.5 \log(1 - e^2) \end{aligned} \quad (2)$$

However, this still requires the assumption that the spin axis of star Aa is aligned with the axis of the orbit ($i_{\text{rot}} = i_{\text{orb}}$), which may or may not be true given the longer orbital period of the binary and its young age.

The top panel of Figure 8 shows that the mean densities of stars Ba and Bb computed in this way, and also that of Aa, seem to agree quite well with predictions from our best-fit 1.6-Myr isochrone, even though they were not used in that fit. It is important to note that in our earlier model comparison there is a certain amount of degeneracy between distance and age because evolutionary tracks are mostly vertical in a diagram of magnitude versus color (or temperature) such as Figure 6; a similarly good agreement with the models can be obtained for a smaller distance if one chooses an older age. On the other hand, the mean stellar densities from eq.(1) and eq.(2) are completely independent of distance, but strongly constrain the age, and are therefore complementary to the brightness measurements. Since the top panel of Figure 8 suggests a somewhat better fit may be had with a slightly younger age, we repeated the comparison incorporating the densities of stars Ba and Bb as additional constraints, though not that of star Aa because of lingering doubts regarding its spin-orbit alignment. The new fit gives an age of 1.4 ± 0.2 Myr, a distance of $D = 133.5_{-6.5}^{+6.0}$ pc, and inclination angles for the binaries of $i_A = 70.5_{-3.5}^{+4.5}$ deg and $i_B = 57.0 \pm 2.5$ deg, which are not very different from our previous results. This new best-fit isochrone is shown with the density measurements in the bottom panel of Figure 8. The agreement with the flux measurements is not significantly altered. The uncertainties are now smaller, especially for the distance and age, because

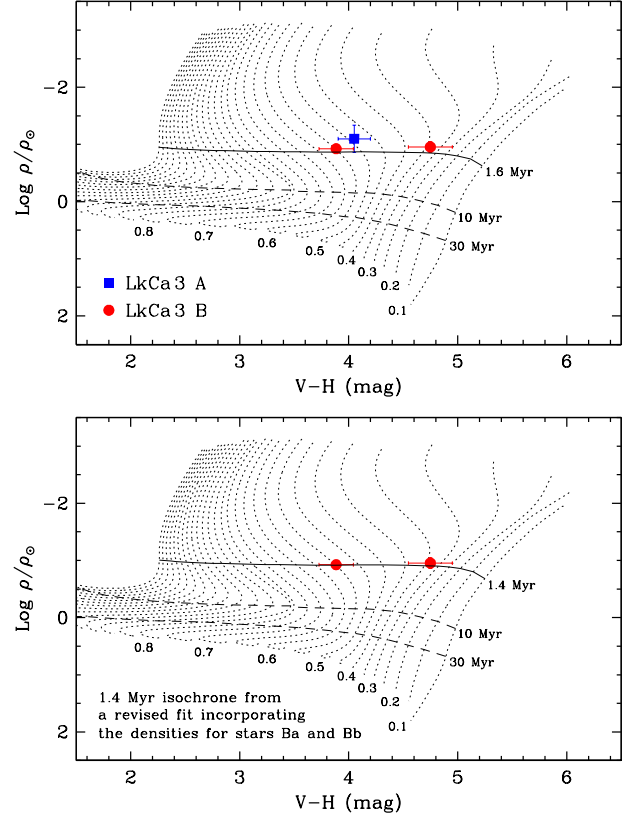


FIG. 8.— *Top*: Mean densities for stars Aa, Ba, and Bb based on our $v \sin i$ measurements and adopted rotation periods (see text), compared against the same PMS stellar evolution models from the Dartmouth series shown in Figure 6. *Bottom*: As above, with the best-fit isochrone changed to 1.4 Myr from a new fit incorporating the mean densities of stars Ba and Bb.

use of the densities suppresses the age-distance correlation to a significant degree. This is illustrated graphically in Figure 9. The masses of the stars do not change appreciably, but the radii are now somewhat larger because of the slightly younger age (approximately $1.63 R_{\odot}$ for stars Aa and Ba, and $1.27 R_{\odot}$ for Ab and Bb).

5.2. Exploring different distance estimates

Given the multiple constraints on the models afforded by the observations for LkCa 3, we investigated the possibility that the data might enable us to determine the distance to each binary independently, and perhaps disprove our assumption that LkCa 3 A and B are physically associated. Because some of these constraints including the flux ratios and combined magnitudes involve properties of both binaries, it is not possible to carry out completely independent solutions as the individual colors and magnitudes of the binary components are strongly correlated. Instead, we performed a joint solution involving all four stars as before, but we allowed the distance as well as the age and inclination angle of each binary to vary independently, for a total of six free parameters. However, since the mean stellar density constraint is applied only for stars Ba and Bb, the parameters for LkCa 3 A are more poorly determined, and the distances turn out to be indistinguishable within their formal errors: 142_{-21}^{+22} pc for LkCa 3 A, and $135.5_{-9.6}^{+7.5}$ pc for LkCa 3 B. The ages are $0.9_{-0.3}^{+0.8}$ Myr and $1.6_{-0.2}^{+0.4}$ Myr, and the inclination angles

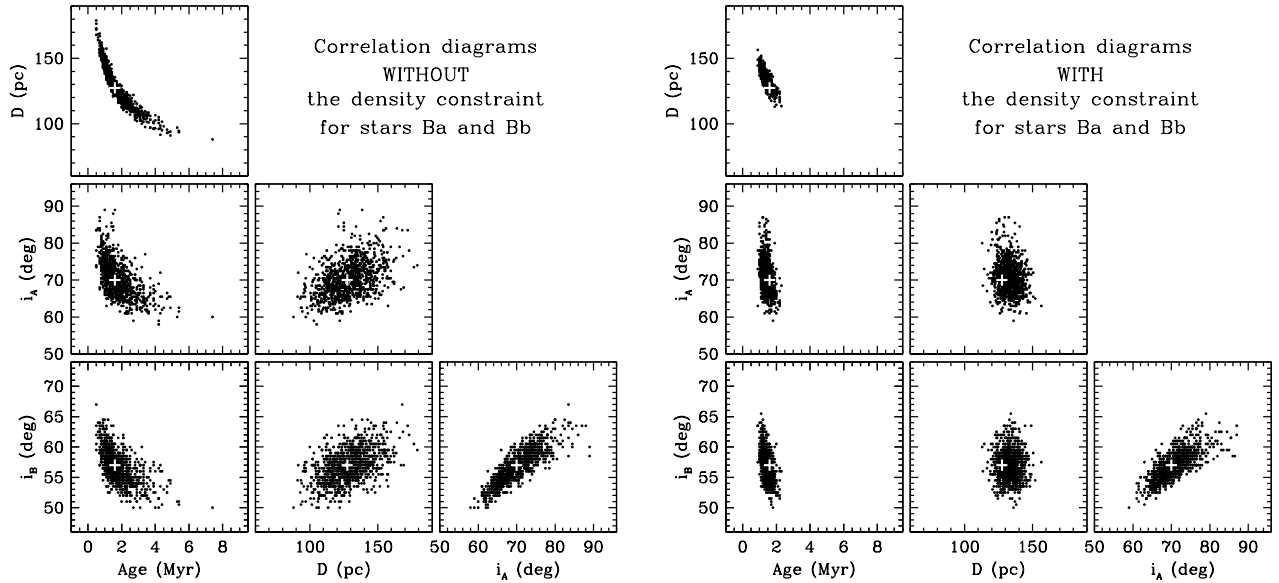


FIG. 9.— *Left:* Correlation diagrams between age, distance, and the orbital inclination angles of LkCa 3 A and B resulting from our Monte Carlo simulations to find the best fit between the observations and the Dartmouth models. Crosses mark the best fit parameters. These simulations did not make use of the constraint on the stellar densities of stars Ba and Bb that comes from $v \sin i$. *Right:* The same diagrams from simulations now including the density constraints. This largely removes the degeneracies between various parameters, particularly age and distance.

$i_A = 76.6^{+17.4}_{-6.7}$ deg and $i_B = 55.5^{+2.6}_{-2.0}$ deg, respectively. The parameters for LkCa 3 B are close to those reported previously, as expected from the strength of the density constraint.

6. DISCUSSION

LkCa 3 is perhaps a unique case among PMS stars because of the many observational constraints available for the comparison with stellar evolution models, and the fact that we know these properties for four stars in the same system that are presumably coeval. Beyond the effective temperatures and relative fluxes in several passbands, which are sometimes available for other PMS binaries, in LkCa 3 we have also dynamical information in the form of minimum masses for all stars, and the additional constraint from the mean densities for at least two of the components. While the inferred age and particularly the distance are in excellent agreement with expectations for the Taurus-Auriga complex, these results are specific to the Dartmouth models of Dotter et al. (2008). As a test we repeated the exercise with the earlier but widely used series of Lyon models by Baraffe et al. (1998), which differ in the degree of convection assumed, among other physical ingredients. While the Dartmouth models adopt a mixing length parameter of $\alpha_{\text{ML}} = 1.938$ in units of the pressure scale height that yields a good fit to the solar properties, the publicly available Lyon models for low-mass stars use $\alpha_{\text{ML}} = 1.0$. With these models we obtained a slightly older age of $2.4^{+0.1}_{-0.4}$ Myr and a rather different distance of 194^{+12}_{-6} pc for LkCa 3 that seems implausibly high for Taurus-Auriga. The quality of the fit is generally worse, giving a χ^2 value of ~ 65 as opposed to ~ 32 . A few of the measurements deviate by more than 3σ , which was not the case before, although there is no obvious pattern in the $O - C$ residuals (see Figure 10) except that the predicted temperatures seem consistently higher than observed. The inclination angles of the two binaries come out considerably smaller

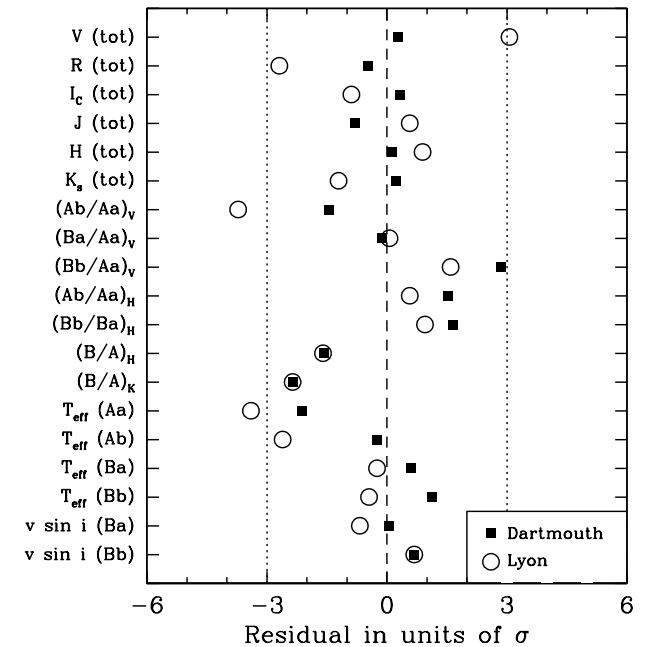


FIG. 10.— $O - C$ residuals from the fits of the PMS isochrones to the observations of LkCa 3 in Table 4, for both the Dartmouth and Lyon models. The residuals are plotted in units of the corresponding uncertainty of the measurement (σ) as given in that table. The dotted lines mark the $\pm 3\sigma$ deviations.

($i_A = 47.5 \pm 1.0$ deg and $i_B = 41.0 \pm 1.0$ deg), resulting in component masses that are essentially a factor of two larger than our previous results. The primaries of the two binaries become $\sim 1 M_\odot$ stars, which seems unreasonably high for an M star.

A more direct comparison between the Dartmouth and Lyon models is illustrated in Figure 11, for two representative solar-metallicity isochrones of 1 Myr and 10 Myr. The differences are shown both in the theoretical plane of $\log L/L_\odot$ vs. T_{eff} and in the observational plane of

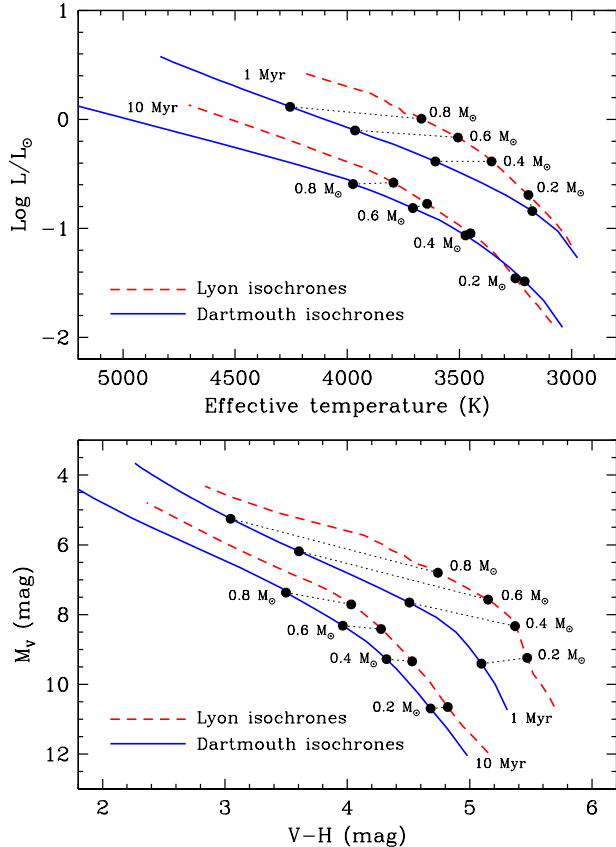


FIG. 11.— Comparison of young solar-metallicity isochrones from the Dartmouth series of Dotter et al. (2008) with similar models from the Lyon series of Baraffe et al. (1998) that use $\alpha_{\text{ML}} = 1.0$, highlighting the significant differences. *Top*: Models in the theoretical $\log L$ versus T_{eff} plane for ages of 1 and 10 Myr. Selected masses are indicated along each isochrone. *Bottom*: Same isochrones as above, represented in the observational plane of M_V versus $V - H$ color.

M_V vs. $V - H$ employed earlier in this work. Points with equal mass on both sets of models are connected with dotted lines. Several features are noteworthy. The Lyon models of Baraffe et al. (1998) appear systematically higher in the diagrams, particularly at 1 Myr, explaining the larger distance obtained. While the bolometric luminosities are similar in both models at a given mass, the temperatures are higher in the Dartmouth series, increasingly so for larger masses. In the observational plane there are large differences in color of nearly 2 mag for $M = 0.8 M_{\odot}$, which are partly attributable to the temperature differences just mentioned, and perhaps also to the color/temperature transformations used in each model. This is the reason for the much larger masses we obtain for LkCa 3 when using the Baraffe et al. (1998) models. All of these differences are seen to be larger at younger ages, which is where the models are most sensitive to initial conditions, and also where the calculations are known to be less reliable (see, e.g., Tout et al. 1999; Siess 2001; Baraffe et al. 2002). We note also that neither set of models incorporates the effects of magnetic fields, which are ubiquitous among PMS stars and have been shown to have a significant impact on theoretical predictions for young stars (e.g., D’Antona et al. 2000). The same has been found more generally for late-type

active main-sequence stars (e.g., Mullan & MacDonald 2001; Chabrier et al. 2007; Feiden & Chaboyer 2012).

The popularity of the Lyon models with $\alpha_{\text{ML}} = 1.0$ for PMS stars and the relatively infrequent use the Dartmouth models have had so far in this area of research motivate us to examine these discrepancies in more detail below, for the impact they may have on our knowledge of young stars.

6.1. The discrepancies with the Lyon models

The poor performance of the Lyon models of Baraffe et al. (1998) in the case of LkCa 3 may seem surprising given that they have been employed in numerous studies since their appearance, and have even been used to help define the temperature scale for late-type PMS stars (see below). On relatively few occasions have difficulties with these models been documented in the young-star literature (for examples see Luhman & Reike 1998; Hillenbrand & White 2004). This may have to do with the nature and large number of observational constraints for LkCa 3, in contrast with the typical situation for young stars. A somewhat similar case to LkCa 3 in terms of the strength of the observational constraints is that of GG Tau, which is another hierarchical quadruple PMS system comprised of two visual binaries in the Taurus-Auriga star-forming region. This system is often regarded as a benchmark for testing evolutionary calculations for young stars, and the observations for GG Tau are generally considered to support the validity of the Lyon models, in apparent contradiction with our findings for LkCa 3.

For GG Tau the individual spectral types (K7+M0 and M5+M7) and luminosities (for an assumed distance of 140 pc) are known for all four components from the work of White et al. (1999). Additionally, the total mass of one of the binaries (GG Tau A) has been estimated from measurements of the orbital velocities of the circumbinary disk ($M_{\text{Aa+Ab}} = 1.28 \pm 0.07 M_{\odot}$; Dutrey et al. 1994; Guilloteau et al. 1999). As in LkCa 3, the four stars in GG Tau form a “mini-cluster” of sorts (on the assumption that they are coeval), which means they provide an unusually strong constraint on stellar evolution theory because a successful model must be able to reproduce the properties of all four components at a single age. This was exploited by White et al. (1999) to test the Lyon models, among others, and in the process to establish a conversion between spectral types and effective temperatures for late-type PMS stars, which has been a persistent source of uncertainty in the field.

The authors showed that the solar-metallicity Lyon models with $\alpha_{\text{ML}} = 1.0$, which are the same ones we used for LkCa 3, provide a good match to the effective temperatures and luminosities of all four stars in GG Tau (see their Fig. 6), but yield a predicted total mass for GG Tau A of $2.00 \pm 0.17 M_{\odot}$ that is considerably larger than observed. Thus, these models fail as in the case of LkCa 3. The temperatures in this analysis were converted from spectral types, but were allowed some freedom for the cooler stars Ba and Bb in order to produce the best fit, which resulted in an implied temperature scale for the SpT/ T_{eff} conversion that is intermediate between dwarfs and giants. The two scales converge for the hotter stars Aa and Ab, which were not adjusted separately. White et al. (1999) also tested Lyon mod-

els computed with a higher mixing length parameter of $\alpha_{\text{ML}} = 1.9$ appropriate for the Sun. These were found to produce a similarly good agreement with the temperatures (readjusted for Ba and Bb) and luminosities, and a lower mass for GG Tau A of $1.46 \pm 0.10 M_{\odot}$ that is in better accord with the dynamically measured value. Very similar conclusions were reached by Luhman (1999) for the $\alpha_{\text{ML}} = 1.9$ models from Lyon, apparently lending support to their accuracy.

We point out, however, that the $\alpha_{\text{ML}} = 1.9$ models employed by the above authors are actually a “hybrid”, since published tabulations from the Lyon group with this mixing length parameter only reach down to $0.6 M_{\odot}$. Below this mass the authors reverted to the Baraffe et al. (1998) models with $\alpha_{\text{ML}} = 1.0$, on the assumption that variations in α_{ML} are inconsequential under $0.6 M_{\odot}$ (Chabrier & Baraffe 1997; Baraffe et al. 1998). As it turns out, 1 Myr models for the two values of α_{ML} have about the same luminosity at this mass, but temperatures that differ significantly by some 230 K, with the $\alpha_{\text{ML}} = 1.9$ calculations being hotter (see also Weinberger et al. 2013). Both White et al. (1999) and Luhman (1999) were then forced to artificially connect the $\alpha_{\text{ML}} = 1.0$ isochrones below $0.6 M_{\odot}$ in some smooth fashion with the $\alpha_{\text{ML}} = 1.9$ isochrones at some mass above $0.6 M_{\odot}$ in order to bridge the discontinuity, which results in a kink at $0.6 M_{\odot}$ and an unsmooth and likely unphysical change in stellar properties across the boundary.

This situation is less than ideal because the $\alpha_{\text{ML}} = 1.9$ models were computed with a helium abundance Y appropriate for the Sun that is not the same as that assumed for the $\alpha_{\text{ML}} = 1.0$ models. A larger Y for these young ages (as in the $\alpha_{\text{ML}} = 1.9$ models) typically leads to a lower luminosity at a given temperature, with some dependence on mass, so in a strict sense joining the isochrones is inconsistent. Furthermore, the assumption that the models become insensitive to the mixing length parameter below about $0.6 M_{\odot}$ is not necessarily valid at early ages for stellar models with low surface gravities and cool temperatures (Baraffe et al. 2002), and may only hold true for much lower masses (see also Burrows et al. 1989; D’Antona & Mazzitelli 1994; Luhman & Reike 1998). Indeed, a comparison of published Lyon models with $\alpha_{\text{ML}} = 1.9$ and $\alpha_{\text{ML}} = 1.0$ shows that the difference in effective temperature at a fixed mass of $0.6 M_{\odot}$ rises considerably toward younger ages, from about 60 K at 10 Myr, to 120 K at 3 Myr, and 230 K at 1 Myr, which is the age regime relevant for GG Tau.

This undermines the conclusion that the Lyon models for “ $\alpha_{\text{ML}} = 1.9$ ” used by White et al. (1999) and Luhman (1999) agree with the measurements for GG Tau, as the comparison may not be very meaningful.

Given that the Dartmouth models seem to work well for LkCa3, it is of interest to see how they fare when tested against the observed properties of GG Tau. This comparison is shown in Figure 12, for an age of 1 Myr. The spectral types and luminosities adopted for stars Aa and Ab are those reported by White et al. (1999), and for stars Ba and Bb we used the revised determinations by Luhman (1999). Spectral types were converted to effective temperatures with the intermediate scale of Luhman (1999) for Ba and Bb, and the dwarf scale for Aa and Ab

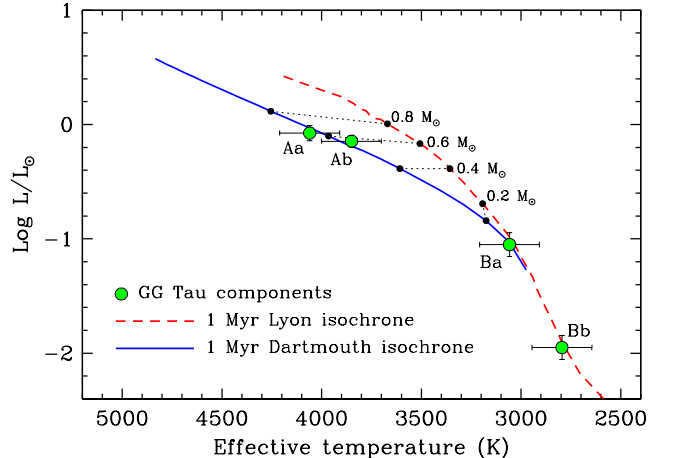


FIG. 12.— Bolometric luminosities and effective temperatures for the components of the quadruple PMS system GG Tau (White et al. 1999; Luhman 1999) compared against 1-Myr solar-metallicity isochrones from the Dartmouth series of Dotter et al. (2008) and the Lyon series of Baraffe et al. (1998) for $\alpha_{\text{ML}} = 1.0$, as displayed in the top panel of Figure 11. The Lyon model extends to lower masses than available in the Dartmouth calculations. Reference masses (small circles) are labeled along both models and are connected with dotted lines.

since the difference with the giant scale is insignificant at these earlier spectral types.⁸ The temperatures were assigned a conservative uncertainty of 150 K, corresponding approximately to a spectral type error of one subtype.

In Figure 12 star Bb is outside the range of masses covered by the Dartmouth models, but there is excellent agreement for the other three components of GG Tau. The dynamical mass estimate for GG Tau A is also well reproduced by these models: the sum of the inferred masses of stars Aa and Ab is $1.19 \pm 0.06 M_{\odot}$, to be compared with the measured value of $1.28 \pm 0.07 M_{\odot}$. The individual masses we derive from the Dartmouth models are $M_{\text{Aa}} = 0.63 \pm 0.05 M_{\odot}$, $M_{\text{Ab}} = 0.56 \pm 0.04 M_{\odot}$, and $M_{\text{Ba}} = 0.15 \pm 0.02 M_{\odot}$.

We note that the SpT/ T_{eff} conversion of Luhman (1999) used in this comparison was established largely using GG Tau itself (specifically, the Ba and Bb components) along with the hybrid “ $\alpha_{\text{ML}} = 1.9$ ” models from Lyon. Using this to test the Dartmouth models may therefore seem to be inconsistent. However, as seen in Figure 12, the Lyon and Dartmouth isochrones converge near star Ba (slightly under $0.2 M_{\odot}$), so the fact that the Dartmouth model is able to match the temperature of this star is not surprising. Whether it would also be able to reproduce the temperature of the Bb component using the same SpT/ T_{eff} conversion, if the calculations were extended to lower masses, remains to be seen.

We conclude from the above that, as in the case of LkCa3, the available constraints for the quadruple system GG Tau favor the PMS Dartmouth models over those from Lyon with $\alpha_{\text{ML}} = 1.0$, at least at these young ages. It is quite possible, however, that the Lyon models with the higher value of $\alpha_{\text{ML}} = 1.9$, if they were available for masses below $0.6 M_{\odot}$, might also perform well, although this cannot be verified at the moment. A sec-

⁸ Luhman et al. (2003a) reported a minor revision of the temperature scale that has a negligible effect on our conclusions, as it implies only a 10 K reduction in T_{eff} for star Bb.

ond conclusion we may draw is that the Dartmouth models do not appear to be inconsistent with the SpT/ T_{eff} prescription advocated by Luhman (1999), in which a dwarf-like temperature scale is adopted for young stars earlier than M0 and an intermediate scale for later-type stars, although further observational constraints between M1 and M5 are required to confirm this.

Based on the examples of GG Tau and LkCa 3 we would expect that in other cases the use of the Dartmouth models instead of the $\alpha_{\text{ML}} = 1.0$ Lyon models for PMS stars would result in generally smaller inferred masses, and slightly younger ages, although this will depend to some extent on the constraints available.

7. FINAL REMARKS

The quadruple system LkCa 3 presented here provides an unusually stringent test of PMS evolution models that appears even stronger than the classical case of GG Tau. In both systems what makes the constraint on theory so strong is the dynamical mass information, and in LkCa 3 the additional estimates of the mean stellar densities for two of the components. While young clusters, associations, and larger star-forming regions such as IC 348, ϵ Cha, η Cha, Chamaeleon I, Taurus (Luhman 1999, 2004a,b; Luhman et al. 2003a,b) and many others do provide some ability to test models from the fact that they are coeval populations, and can also help to establish the SpT/ T_{eff} relation for PMS stars, the constraints they afford are not as tight because of the often large scatter of the measurements in the H-R diagram, and the lack of information on mass.

The Dartmouth models of Dotter et al. (2008), with their consistent physics across the entire mass range, are strongly favored by the observations of LkCa 3 and GG Tau over the Lyon models with $\alpha_{\text{ML}} = 1.0$. In retrospect, the performance of the latter models when confronted with the challenge of multiple complementary constraints for the same stellar system is not entirely surprising, as there is no obvious physical reason why the mixing length parameter should have precisely that value. The present study has shown that the Dartmouth models are also preferred over the hybrid Lyon models with “ $\alpha_{\text{ML}} = 1.9$ ” considered by White et al. (1999), Luhman (1999), and others, which *do not* use consistent physics.

Other than the present work, relatively few tests of the Dartmouth models for pre-main sequence stars have been reported in the literature, but are highly desirable to strengthen our confidence in the predictive power of these calculations. Binary and multiple systems are especially suited for this, and other information for these or other young objects can be extremely helpful such

as trigonometric parallaxes (which the GAIA space mission is expected to supply in the near future), angular diameters, and chemical analyses including determinations of the lithium abundance. For example, although strong Li I $\lambda 6707$ in absorption is present in LkCa 3, the multiplicity of the system has so far made a quantitative interpretation of those measurements impossible. The recent high-resolution spectroscopic study by Nguyen et al. (2012) did not report Li measurements, but a graphical representation of the Li region for their four spectra shows several components which we can now identify from our orbital solutions. Stars Aa, Ba, and Bb all exhibit the line in absorption, though we see no sign of star Ab, the faintest one of the four. With knowledge of the flux ratios from our work, it should now be possible to re-analyze the original Nguyen et al. (2012) spectra and derive Li abundances for at least three of the stars, properly corrected for the light contribution from the other components. This could serve as an important additional constraint on stellar evolution models.

We thank the anonymous referee for interesting suggestions, as well as I. Baraffe and R. White for helpful exchanges about stellar evolution models. The spectroscopic observations at the CfA were obtained with the able assistance of P. Berlind, R. Davis, L. Hartmann, E. Horine, A. Milone, and J. Peters. We are grateful to R. Davis for maintaining the CfA echelle database over the years. We also thank C. Beichman for the opportunity to obtain an additional NIRSPEC spectrum on the night of UT 2010 November 22. We thank the staff at Keck Observatory for their superb support. Data presented herein were obtained at the W. M. Keck Observatory from telescope time allocated to the National Aeronautics and Space Administration through the agency’s scientific partnership with the California Institute of Technology and the University of California. LP acknowledges support from NASA Keck PI Data Award administered by NExSci (semesters 2003B and 2004A). Keck telescope time was also granted by NOAO, through the Telescope System Instrumentation Program (TSIP). TSIP was funded by the NSF. The Observatory was made possible by the generous financial support of the W. M. Keck Foundation. We recognize the Hawaiian community for the opportunity to conduct these observations from the summit of Mauna Kea. This work was partially supported by NSF grants AST-1007992 to GT and AST-1009136 to LP. The research has made use of NASA’s Astrophysics Data System Abstract Service, and of the SIMBAD and VizieR databases, operated at the CDS, Strasbourg, France.

REFERENCES

- Amores, E. B., & Lepine, J. R. D. 2005 AJ, 130, 659
 Andrews, S. M., & Williams, J. P. 2005, ApJ, 631, 1134
 Baraffe, I., Chabrier, G., Allard, F., & Hauschildt, P. H. 1998, A&A, 337, 403
 Baraffe, I., Chabrier, G., Allard, F., & Hauschildt, P. H. 2002, A&A, 382, 563
 Bate, M. R. 2009, MNRAS, 392, 590
 Bouvier, J., Covino, E., Kovo, O., Martın, E. L., Matthews, J. M., Terranegra, L., & Beck, S. C. 1995, A&A, 299, 89
 Boyajian, T. S., von Braun, K., van Belle, G. et al. 2012, ApJ, 757, 112
 Briceno, C., Luhman, K. L., Hartmann, L., Stauffer, J. R., & Kirkpatrick, J. D. 2002, ApJ, 580, 317
 Burrows, A., Hubbard, W. B., & Lunine, J. I. 1989, ApJ, 345, 939
 Cardelli, J. A., Clayton, G. C., & Mathis, J. S. 1989, ApJ, 345, 245
 Chabrier, G., Gallardo, J., & Baraffe, I. 2007, A&A, 472, L17
 Chabrier, G., & Baraffe, I. 1997, A&A, 327, 1039
 Covino, E., Melo, C., Alcala, J. M., Torres, G., Fernandez, M., Frasca, A., & Paladino, R. 2001, A&A, 375, 130

- Cutri, R. M. et al. 2003, 2MASS All Sky Catalog of Point Sources, NASA/IPAC Infrared Science Archive, <http://irsa.ipac.caltech.edu/applications/Gator/>
- D'Antona, F., & Mazzitelli, I. 1994, *ApJS*, 90, 467
- D'Antona, F., Ventura, P., & Mazzitelli, I. 2000, *ApJ*, 543, L77
- Dotter, A., Chaboyer, B., Jevremović, D., Kostov, V., Baron, E., & Ferguson, J. W. 2008, *ApJS*, 178, 89
- Drimmel, R., Cabrera-Lavers, A., & López-Corredoira, M. 2003, *A&A*, 409, 205
- Duchêne, G., & Kraus, A. 2013, *ARA&A*, in press (arXiv:1303.3028)
- Dutrey, A., Guilloteau, S., & Simon, M. 1994, *A&A*, 286, 149
- Dutrey, A., Guilloteau, S., Duvert, G., Prato, L., Simon, M., Schuster, K., & Ménard, F. 1996, *A&A*, 309, 493
- Feiden, G. A., & Chaboyer, B. 2012, *ApJ*, 761, 30
- Ghez, A., Neugebauer, G., & Matthews, K. 1993, *AJ*, 106, 2005
- Gómez, M., Hartmann, L., Kenyon, S. J., & Hewett, R. 1993, *AJ*, 105, 1927
- Grankin, K. N., Bouvier, J., Herbst, W., & Melnikov, S. Y. 2008, *A&A*, 479, 827
- Gray, D. F. 2005, *The Observation and Analysis of Stellar Photospheres* (Cambridge: CUP), p. 506
- Guenther, E. W., Esposito, M., Mundt, R., Covino, E., Alcalá, J. M., Cusano, J. M., Stecklum, B. 2007, *A&A*, 467, 1147
- Guilloteau, S., Dutrey, A., & Simon, M. 1999, *A&A*, 348, 570
- Hakkila, J., Myers, J. M., Stidham, B. J., & Hartmann, D. H. 1997, *AJ*, 114, 2043
- Hartmann, L. W., Soderblom, D. R., & Stauffer, J. R. 1987, *AJ*, 93, 907
- Herbig, G. H., Vrba, F. J., & Rydgren, A. E. 1986, *AJ*, 91, 575
- Hillenbrand, L. A., & White, R. J. 2004, *ApJ*, 604, 741
- Hut, P. 1981, *A&A*, 99, 126
- Kenyon, S. J., & Hartmann, L. 1995, *ApJS*, 101, 117
- Latham, D. W. 1985, in *IAU Coll. 88, Stellar Radial Velocities*, eds. A. G. D. Philip & D. W. Latham (Schenectady: L. Davis), 21
- Latham, D. W. 1992, in *IAU Coll. 135, Complementary Approaches to Double and Multiple Star Research*, ASP Conf. Ser. 32, eds. H. A. McAlister & W. I. Hartkopf (San Francisco: ASP), 110
- Leinert, Ch., Zinnecker, H., Weitzel, N., Christou, J., Ridgway, S. T., Jameson, Haas, M., & Lenzen, R. 1993, *A&A*, 278, 129
- Loinard, L., Torres, R. M., Mioduszewski, A. J., et al. 2007, *ApJ*, 671, 546
- Lucy, L. B., & Sweeney, M. A. 1971, *AJ*, 76, 544
- Luhman, K. L. 1999, *ApJ*, 525, 466
- Luhman, K. L. 2004a, *ApJ*, 602, 816
- Luhman, K. L. 2004b, *ApJ*, 616, 1033
- Luhman, K. L., Briceño, C., Stauffer, J. R., et al. 2003b, *ApJ*, 590, 348
- Luhman, K. L., & Reike, G. H. 1998, *ApJ*, 497, 354
- Luhman, K. L., Stauffer, J. R., Muench, A. A., Rieke, G. H., Lada, E. A., Bouvier, J., & Lada, C. J. 2003a, *ApJ*, 593, 1093
- Mace, G. N., Prato, L., Torres, G., et al. 2012, *AJ*, 144, 55
- Mathieu, R. D. 1994, *ARA&A*, 323, 465
- Mathieu, R. D., Baraffe, I., Simon, M., Stassun, K. G., & White, R. 2007, in *Protostars and Planets V*, eds. B. Reipurth, D. Jewitt & K. Keil (Tucson: Univ. of Arizona Press), 411
- Mathieu, R. D., Latham, D. W., Mazeh, T., et al. 1992, *Binaries as Tracers of Star Formation*, ed. A. Duquennoy & M. Mayor (Cambridge: Cambridge Univ. Press), 278
- Mazeh, T. 2008, *EAS Publications Series*, 29, 1
- Mazeh, T., Prato, L., Simon, M., et al. 2002, *ApJ*, 564, 1007
- McCabe, C., Ghez, A. M., Prato, L., Duchêne, G., Fisher, R. S., & Telesco, C. 2006, *ApJ*, 636, 932
- McLean, I. S. et al. 1998, *Proc. SPIE*, 3354, 566
- McLean, I. S. et al. 2000, *Proc. SPIE*, 4008, 1048
- Meibom, S., & Mathieu, R. D. 2005, *ApJ*, 620, 970
- Melo, C. H. F., Covino, E., Alcalá, J. M., & Torres, G. 2001, *A&A*, 378, 898
- Melo, C. H. F. 2003, *A&A*, 410, 269
- Mullan, D. J., & MacDonald, J. 2001, *ApJ*, 559, 353
- Nguyen, D. C., Brandeker, A., van Kerkwijk, M. H., & Jayawardhana, R. 2012, *ApJ*, 745, 119
- Norton, A. J. et al. 2007, *A&A*, 467, 785
- Palla, F., & Stahler, S. W. 2002, *ApJ*, 581, 1194
- Prato, L. 2007, *ApJ*, 657, 338
- Prato, L., Simon, M., Mazeh, T., McLean, I. S., Norman, D., & Zucker, S. 2002a, *ApJ*, 569, 863
- Prato, L., Simon, M., Mazeh, T., Zucker, S., & McLean, I. S. 2002b, *ApJ*, 579, L99
- Roberts, D. H., Lehar, J., & Dreher, J. W. 1987, *AJ*, 93, 968
- Rojas-Ayala, B., Covey, K. R., Muirhead, P. S., & Lloyd, J. P. 2012, *ApJ*, 748, 93
- Rosero, V., Prato, L., Wasserman, L. H., & Rodgers, B. 2011, *AJ*, 141, 13
- Rousselot, P., Lidman, C., Cuby, J. G., & Moreels, G. 2000, *A&A*, 354, 1134
- Schlegel, D. J., Finkbeiner, D. P., & Davis, M. 1998, *ApJ*, 500, 525
- Siess, L. 2001, *From Darkness to Light: Origin and Evolution of Young Stellar Clusters*, ASP Conf. Ser. 243, eds. T. Montmerle & P. André (San Francisco: ASP), 581
- Simon, M. 2008, *The Power of Optical/IR Interferometry: Recent Scientific Results and 2nd Generation*, eds. A. Richichi, F. Delplancke, F. Paresche & A. Chelli (Garching: Springer), 227
- Simon, M., & Prato, L. 1995, *ApJ*, 450, 824
- Simon, M., Schaefer, G. H., Prato, L., Ruiz-Rodríguez, D., Karnath, N., Franz, O. G., & Wasserman, L. H. 2013, *ApJ*, in press
- Stassun, K. G., Mathieu, R. D., Mazeh, T., & Vrba, F. J. 1999, *AJ*, 117, 2941
- Stassun, K. G., Mathieu, R. D., Vrba, F. J., Mazeh, T., & Henden, A. 2001, *AJ*, 121, 1003
- Torres, G., Neuhäuser, R., & Guenther, E. W. 2002, *AJ*, 123, 1701
- Torres, G., Latham, D. W., & Stefanik, R. P. 2007, *ApJ*, 662, 602
- Torres, R. M., Loinard, L., Mioduszewski, A. J., & Rodríguez, L. F. 2007, *ApJ*, 671, 1813
- Torres, R. M., Loinard, L., Mioduszewski, A. J., & Rodríguez, L. F., 2009, *ApJ*, 698, 242
- Torres, R. M., Loinard, L., Mioduszewski, A. J., et al. 2012, *ApJ*, 747, 18
- Tout, C. A., Livio, M., & Bonnell, I. A. 1999, *MNRAS*, 310, 360
- Weinberger, A. J., Anglada-Escudé, G., & Boss, A. P. 2013, *ApJ*, 762, 118
- White, R. J., & Guez, A. M. 2001, *ApJ*, 556, 265
- White, R. J., & Guez, A. M., Reid, I. N., & Schultz, G. 1999, *ApJ*, 520, 811
- Witte, M. G., & Savonije, G. J. 2002, *A&A*, 386, 222
- Wizinowich, P. L., Acton, D. S., Lai, O. et al. 2000, *Proc. SPIE*, 4007, 2
- Woitás, J., Koehler, R., & Leinert, Ch. 2001a, *A&A*, 369, 249
- Woitás, J., Leinert, Ch., & Koehler, R. 2001b, *A&A*, 376, 982
- Xiao, H. Y., Covey, K. R., Rebull, L., Charbonneau, D., Mandushev, G., O'Donovan, F., Slesnick, C., & Lloyd, J. P. 2012, *ApJS*, 202, 7
- Yelda, S., Lu, J. R., Ghez, A. M., et al. 2010, *ApJ*, 725, 331
- Zahn, J. P., & Bouchet, L. 1989, *A&A*, 223, 112
- Zucker, S., & Mazeh, T. 1994, *ApJ*, 420, 806
- Zucker, S., Torres, G., & Mazeh, T. 1995, *ApJ*, 452, 863